Available online at www.sciencedirect.com
SCIENCE DIRECT
Journal of Power Sources 158 (2006) 535–542
JOURNAL OF POWER SOURCES
www.elsevier.com/locate/jpowsour

Thermal behavior of small lithium-ion battery during rapid charge and discharge cycles

Kazuo Onda*, Takamasa Ohshima, Masato Nakayama, Kenichi Fukuda, Takuto Araki

Department of Electrical and Electronic Engineering, Toyohashi University of Technology, 1-1 Hibarigaoka, Tenpaku-cho, Toyohashi-shi, Aichi-ken 441-8580, Japan

Received 12 July 2005; received in revised form 25 August 2005; accepted 30 August 2005
Available online 19 October 2005

Abstract

The secondary batteries for electric vehicles (EV) generate much heat during rapid charge and discharge cycles at current levels exceeding the batteries' rating, such as when the EV quickly starts consuming battery power or when recovering inertia energy during sudden stops. During these rapid charge and discharge cycles, the cell temperature may increase above allowable limits. We calculated the temperature rise of a small lithium-ion secondary battery during rapid charge and discharge cycles. The heat-source factors were measured again by the methods described in our previous study, because the performance of the battery reported here has been improved, showing lower overpotential resistance. Battery heat capacity was measured by a twin-type heat conduction calorimeter, and determined to be a linear function of temperature. Further, the heat transfer coefficient, measured again precisely by the method described in our previous study, was arranged as a function of cell and ambient temperatures. The temperature calculated by our battery thermal behavior model using these measured data agrees well with the cell temperature measured by thermocouple during rapid charge and discharge cycles. Also, battery radial temperature distributions were calculated to be small, and confirmed experimentally.

Keywords: Lithium-ion secondary battery; Overpotential resistance; Entropy change; Rapid charge and discharge cycles; Thermal behavior model

1. Introduction

Load leveling between power supply and demand by storing surplus power in nighttime for use during peak demand in daytime is promoted in order to narrow the gap between power demand in daytime and supply in nighttime [1]. Moreover, hybrid and electric vehicles (EV) are becoming more practical in order to alleviate the air pollution arising from the increasing number of automobiles [2]. Many institutions are conducting research and development on secondary lithium-ion batteries, as they have high energy and power densities combined with high charge and discharge efficiencies. Much anticipation therefore surrounds these batteries due to their potential use in power storage and electric vehicles. Rapid charging and discharging at higher current than the battery's rated current are anticipated for the large batteries that will be utilized in these applications. As battery size increases, however, the ratio of heat cooling area to heat generating volume decreases, and as charge/discharge current increases, more heat is generated. The temperature of battery thus rises dramatically, leading to the possibility that temperatures will exceed permissible levels. Additionally, charge/discharge characteristics improve as battery temperature increases. Thus, when temperature is distributed inside the battery, the local cell performance becomes uneven with an inclined current distribution in battery, which becomes a source of localized deterioration. Much has been reported about the materials and structures of batteries, but little has been reported on such thermal behavior of batteries as this paper.

We therefore set out to construct a model for analyzing thermal behavior of large lithium-ion secondary batteries during rapid charge and discharge cycles. First, in a previous study [3], we measured the heat-source terms of overpotential resistance and entropy change, however those measurements was conducted at only a discharge current below the battery's rated current. Using these measured data, battery temperatures were

* Corresponding author. Tel.: +81 532 44 6722; fax: +81 532 44 6728.
E-mail address: onda@eee.tut.ac.jp (K. Onda).

0378-7753/$ – see front matter © 2005 Elsevier B.V. All rights reserved.
doi:10.1016/j.jpowsour.2005.08.049

calculated by a thermal behavior model we constructed, being compared with measured battery temperatures. In that study, the measured and calculated temperatures were mostly in good agreement, and the reliability of our thermal behavior model was verified. For the present study, we attempted to expand the usable range of this model by testing whether or not it is also applicable to rapid charge and discharge cycles exceeding the battery's rated current. Using small lithium-ion secondary batteries with improved characteristics, we again measured the overpotential resistance, entropy change, and a more accurate heat transfer coefficient from the battery to the ambient air. The heat capacity of battery was also measured using a calorimeter. Using these measured data, the battery temperature during rapid charge and discharge cycles was calculated using the thermal behavior model. The numerical battery temperature was compared with the measured temperature of battery cooled under natural convection, showing that the calculated temperature mostly agreed with the measured, as explained below. Moreover, one-dimensional analysis of temperature in the radial direction of battery was performed, confirming that the radial temperature distribution in battery is nearly constant, which was also verified experimentally.

2. Thermal behavior model

2.1. Charge/discharge reaction and heat-source terms in lithium-ion secondary battery

The cell tested here has a positive electrode of lithium cobalt oxide ($LiCoO_2$), a negative electrode of graphite carbon, and an electrolyte of lithium salt dissolved in organic solution. The charge/discharge reactions are written as follows [4]:

$$\text{at positive electrode:} \quad LiCoO_2 \underset{\text{discharge}}{\overset{\text{charge}}{\rightleftarrows}} \square CoO_2 + Li^+ + e^- \tag{1}$$

$$\text{at negative electrode:} \quad \square C_6 + Li^+ + e^- \underset{\text{discharge}}{\overset{\text{charge}}{\rightleftarrows}} LiC_6 \tag{2}$$

$$\text{total cell reaction:} \quad LiCoO_2 + \square C_6 \underset{\text{discharge}}{\overset{\text{charge}}{\rightleftarrows}} \square CoO_2 + LiC_6 \tag{3}$$

where $\square$ represents the vacant site for lithium ions.

The charge and discharge reactions for lithium-ion secondary battery are endothermic and exothermic, respectively. If the battery reaction is ideally reversible, the thermodynamic equation under a constant temperature T and constant pressure [5] yields the following relation:

$$\Delta G = \Delta H - T\,\Delta S \tag{4}$$

where the residual energy at energy conversion between the enthalpy change ΔH of the battery reaction and the electrical work ΔG ($=-nFE_{emf}$) can be compensated by the heat energy of $T\,\Delta S$. The heat Q_S by entropy change ΔS is described by the following equation.

$$Q_S = T_{cell}\,\Delta S \frac{I}{nF} \tag{5}$$

$$\Delta S = -\frac{\partial\,\Delta G}{\partial T_{cell}} = nF\frac{\partial E_{emf}}{\partial T_{cell}} \tag{6}$$

where T_{cell} is battery temperature, I charge/discharge current (defined as positive during charge cycle), F Faraday constant, E_{emf} cell potential for open-circuit, and n the charge number pertaining to the reaction ($n=1$ for a lithium-ion battery). The reaction directions for charge and discharge cycles are opposite to each other, thus Q_S is endothermic during charge cycle and exothermic during discharge cycle.

When electric current flows through the cell, cell voltage V deviates from open-circuit potential V_0 due to electrochemical polarization. The energy loss by this polarization dissipates as heat. This overpotential heat Q_P is described as following equation:

$$Q_P = I(V - V_0) = I^2 R_\eta \tag{7}$$

where Q_P is exothermic during both charge and discharge cycles. When the difference between V and V_0 is expressed as IR_η, Q_P can be determined from the overpotential resistance R_η.

2.2. Thermal behavior model described by a representative temperature

In a case where the model is expressed by a representative temperature T_{cell}, T_{cell} can be described by the following heat-balance equation, which is a relation between the cell heat capacity, Q_S, Q_P, and the transferred heat Q_B to the surroundings,

$$C_{cell}\frac{dT_{cell}}{dt} = Q_P + Q_S - Q_B \tag{8}$$

$$Q_B = Ah(T_{cell} - T_{amb}) \tag{9}$$

where C_{cell} is the heat capacity of cell, t time, T_{amb} ambient temperature, A the total surface area of cell including a cylindrical surface and both ends surfaces, and h the heat transfer coefficient.

If the entire cell is verified to have a uniform temperature during the charge and discharge cycles, it is possible to compare the representative cell temperature, which can be conveniently calculated by Eq. (8), with the measured temperature at cell surface.

2.3. One-dimensional analysis of cell temperature distribution [6]

A radial temperature distribution was calculated in order to estimate temperature distribution of the spirally-wound cylindrical cell during the rapid charge and discharge cycles. First, an equivalent circuit was considered for a cell with spread-out positive and negative electrodes and a electrolyte sheet, assuming the following conditions to calculate the current distribution: (1) the spread-out cell consists of local cells which performance

can be described by the charge and discharge characteristics of a small lithium-ion battery as shown in Section 3; (2) no current flows along the sheet of the active material layer; (3) no current distributes along the cylindrical cell's axis (i.e. in the direction for electrode width) due to its good thermal and electric conductance; and (4) the resistance of current collection leads can be ignored. Based on these assumptions, the current I_1 and I_2 in current collection sheets of the positive and negative electrodes, respectively, and the current density J in electrolyte can be described as following:

$$\frac{\partial V_x}{\partial J}\frac{\partial J}{\partial x} = rI_1 - rI_2 - \frac{\partial V_x}{\partial \mathrm{SOC}}\frac{\partial \mathrm{SOC}}{\partial x} - \frac{\partial V_x}{\partial T_{\mathrm{cell}}}\frac{\partial T_{\mathrm{cell}}}{\partial x} \tag{10}$$

$$\frac{\partial I_1}{\partial x} = -2HJ \tag{11}$$

$$\frac{\partial I_2}{\partial x} = -2HJ \tag{12}$$

$$\mathrm{SOC} = \mathrm{SOC}_i - \int \frac{J}{C_{\mathrm{S}}}\,\mathrm{d}t \tag{13}$$

Here x is the distance from the negative lead along the current collection sheet, SOC the state of charge, and V_x, the cell voltage at x, a function of J, SOC, and T_{cell}. Also, r is the resistance per unit length of current collection sheet, H the sheet width, C_{S} the capacitance per unit area of electrode, and suffix i represents the initial condition.

Next, the spread-out cell is re-wound spirally and the obtained current distribution is used to calculate the radial temperature distribution under the following assumptions: (1) the thermal conductivity of the cell is constant along the radial direction; (2) the temperature distribution along the cell axis is too small to be ignored; (3) the physical properties of cell, such as thermal conductivity and specific gravity, do not change during charge and discharge cycles; and (4) there is no convection of the electrolyte. Based on these assumptions, the radial temperature distribution can be described by the following axi-symmetrical equation of one-dimensional thermal conduction.

$$C_{\mathrm{cell}}\frac{\partial T_{\mathrm{cell}}}{\partial t} = \lambda\left(\frac{\partial^2 T_{\mathrm{cell}}}{\partial R^2} + \frac{1}{R}\frac{\partial T_{\mathrm{cell}}}{\partial R}\right) + (Q'_{\mathrm{S}} + Q'_{\mathrm{P}}) \tag{14}$$

Here, C_{cell} is the heat capacity of cell, λ and R represent the thermal conductivity and the radius of cell, respectively. Q'_{S} and Q'_{P} are the local entropy and overpotential heat, respectively, which are given by dividing Q_{S} of Eq. (5) and Q_{P} of Eq. (7) by the cell volume. The obtained temperature distribution is put into Eq. (10) again until the current and temperature distributions are converged.

3. Measurement of heat-source factors

The battery tested here is a commercially-available, cylindrical lithium-ion battery (Sony-US18650G3 with 1800 mAh rated capacity, 18 mm diameter, and 65 mm length). In order to measure the heat-source factors of cell at a constant temperature similarly to the previous study, a cell was charged and discharged after being wrapped in a thin sheet for electrical insulation and immersed in a water thermostat. In this study as well, before each measurement was taken a cell was charged and discharged twice at the rated condition to erase any previous charge and discharge history. States of charge (SOC) were set at 1.0 and 0.0, respectively, at the end of the rated charge and discharge cycles. Here the rated current is defined as the current to discharge the rated capacity of 1800 mAh in 1 h. The rated charge and discharge cycles are defined here as the charge cycle with constant current of 1C (1.8 A) (xC means the multiple x of the rated current) followed by constant (terminal) voltage of 4.2 V for 3 h, and the discharge cycle with constant current of 0.2C (0.36 A) until terminal voltage of 2.7 V followed by an intermittent time of 3 h.

3.1. Measurement of overpotential resistance

We measured resistance by four measurement methods during rapid charge and discharge cycles at a current even much above the rated level.

3.1.1. Resistance by V–I characteristics

Charging tests at constant currents of 0.2–1.7C were performed at cell temperatures of 20, 30, and 40 °C. In addition, discharging tests at constant currents of 0.2–3.0 °C were performed at cell temperatures of 20, 30, 40, and 50 °C. During both charge and discharge cycles, the higher the current the faster the charge or discharge terminal voltage was reached. This was much notable during charge cycle.

The obtained data of the constant-current charge/discharge tests were converted to the voltage–current (V–I) characteristics as parameter of SOC. The V–I characteristics for charging at 30 °C are shown in Fig. 1. The V–I characteristics are mostly linear, and the slopes give the overpotential resistance $R(V$–$I)$ for each SOC. Here, the slopes can be determined using the following three methods: (1) one by the least squares approximation assuming that the V–I characteristic is, on the whole, a straight line; (2) one by determining the gradient of a V–I characteristic curve for each current; (3) one by the least squares approximation assuming that the V–I characteristic is linear at the rated current or less. The resistances determined by these three methods are compared in Fig. 2.

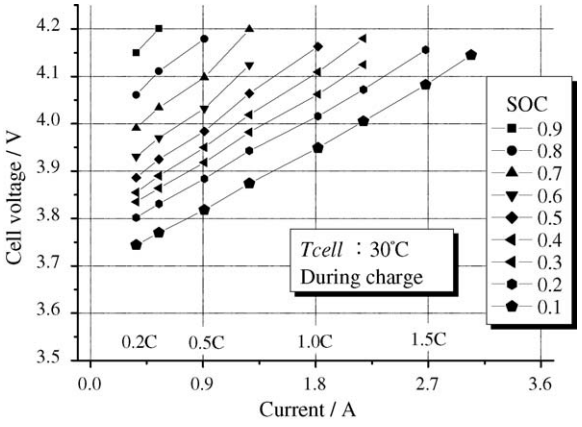

Fig. 1. V–I characteristics with SOC parameter.

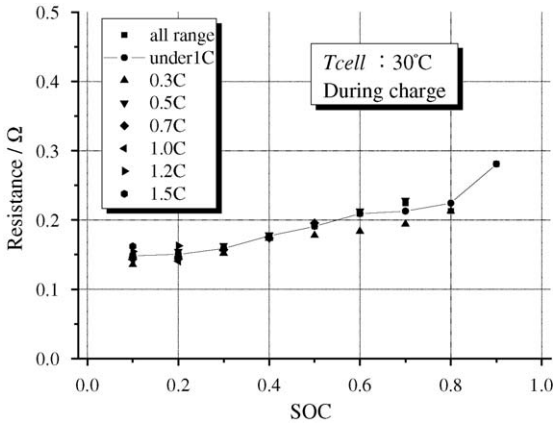

Fig. 2. Comparison of three types of resistances by *V–I* characteristics.

The variance of the resistances determined by the three methods is small and less than 10% for a discharge cycle at 30 °C, based on the slope determined by the third method. Furthermore, all resistances match well at 40 °C and above. When the charge/discharge current becomes larger than the rated, the movement of lithium-ion through the active material is thought to have some diffusive resistance, since the charging voltage is increasing much more than the linearly extrapolated voltage and the discharging voltage is decreasing much less than the linearly extrapolated voltage. So the third resistance, which was obtained from the linear *V–I* characteristic at the rated current or less, can be regarded as the resistance without diffusion of the active material. They are shown in Fig. 3 as the representative resistances for both the charge and discharge cycles. Resistance increases with the progress of charging/discharging and decreases as battery temperature rises. In addition, at a temperature of 30 °C or above during charge cycle, and of 40 °C or above during discharge cycle, there was no change in resistance by temperature. Moreover, Fig. 3 also shows our previous study's resistance (at 40 °C) during discharge cycle, and shows that the present battery resistance is about a half of the previous data. From this it can be seen that the battery's characteristics have been improved.

3.1.2. Resistance by difference between open-circuit voltage (OCV) and cell voltage

Cell voltage V during charge/discharge cycle deviates from the open-circuit voltage V_0. Overpotential resistance R(OCV-CV) can also be obtained by dividing the difference in these voltages by the charge/discharge current. Here, V_0 changes slightly over time just after charging/discharging. In the present study, the battery was adjusted to a given SOC with a 0.2 °C discharge current after being fully charged. The cell voltage after a 21-h stabilization period from the SOC adjusted time was regarded as V_0, which is thought not to affected by the active material diffusion. Fig. 4 compares R(*V–I*) determined in previous section with R(OCV-CV) in this section at 30 °C and 1C. The figure shows that R(OCV-CV) is nearly identical to R(*V–I*) for both charge and discharge cycles, even when battery temperature or charge/discharge current is changed.

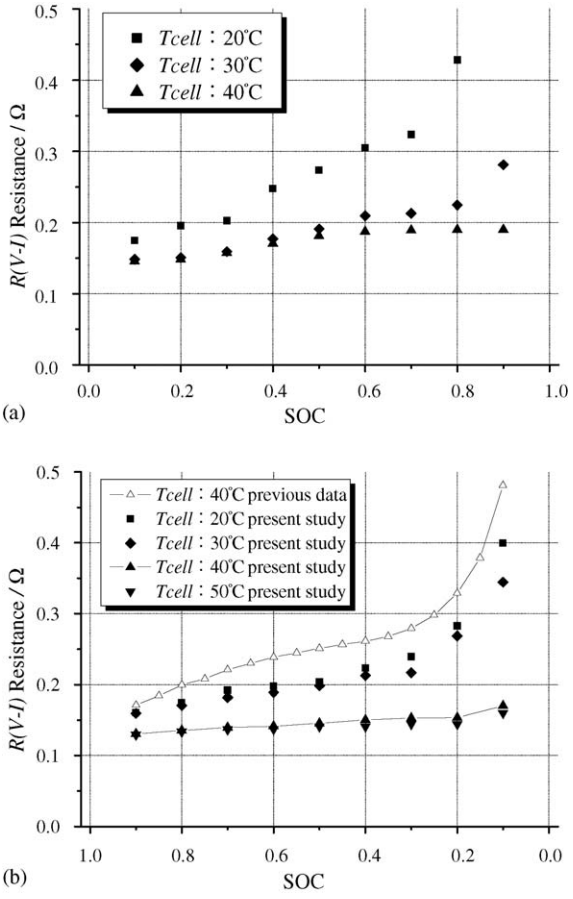

Fig. 3. Overpotential resistance R(*V–I*) by *V–I* characteristics under 1C: (a) during charge; (b) during discharge.

3.1.3. Resistance by intermittent charge/discharge

Overpotential resistance R(60 s) can simply be determined by intermittent charge/discharge (60-s duration). After the battery was fully charged, SOC was dropped in 0.1 increments and R(60 s) by intermittent discharge was determined by dividing the voltage drop $V_{60\,s}$ at 60 s after the start of every discharge by the discharge current. An average SOC was used, however, as SOC changes after 60 s. Measurement by intermittent charge was performed in the same manner.

Fig. 4 also shows R(60 s) at 30 °C and 1C. Even when battery temperature or charge/discharge current is changed, R(60 s) and R(OCV-CV) are nearly identical to R(*V–I*).

3.1.4. Resistance by AC impedance meter

In the field of electrochemistry, they usually use the AC impedance meter to measure battery resistance. Here we also measured overpotential resistance by applying an AC current of 70 mA root mean square (rms) at a frequency range of 20 kHz–25 mHz, using an electrochemical measurement unit (Solartron 1280B). In the previous study, the measured resistance did not depend on discharge current, therefore, resistance was here measured also without any charge/discharge current. Fig. 5 shows the measured Cole–Cole plot. Fig. 4 also shows the real part of the complex impedance as R(AC), neglecting the

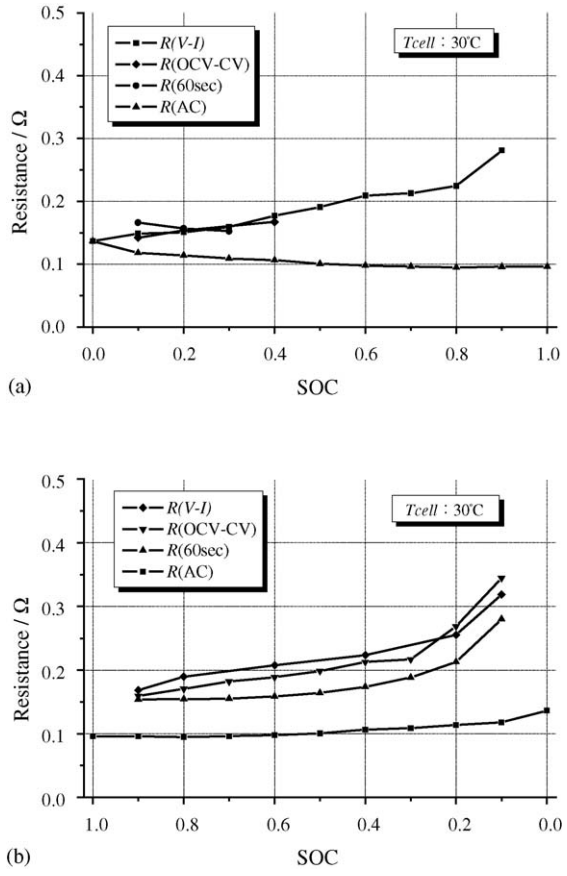

Fig. 4. Comparison of overpotential resistances by four methods: (a) during charge; (b) during discharge.

Warburg impedance by diffusion. The value of R(AC) becomes about a half of R(V–I). Depending on battery as described here, about a half of resistance was again measured similarly to the previous study.

3.2. Measurement of entropy change

Even though the same model of battery as in the previous study was tested, the improvements of battery's performance

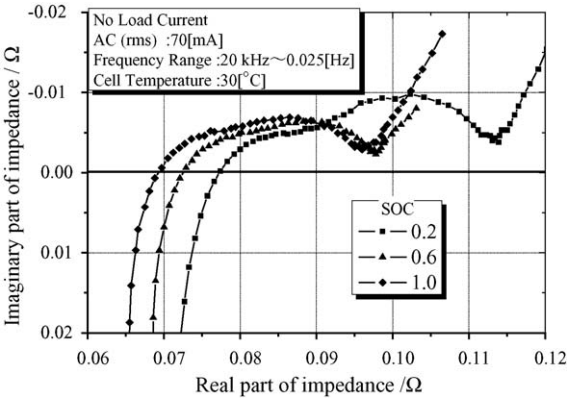

Fig. 5. AC impedance measured for battery.

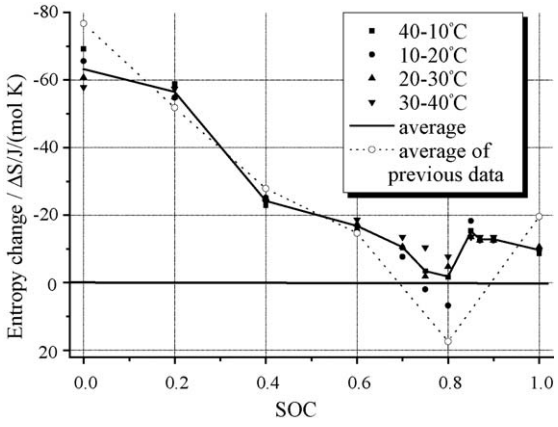

Fig. 6. Measured entropy change for SOC and cell temperature.

made us to re-measure the additional heat-source term, entropy change. Identical to before, the battery was regulated to a given SOC then first immersed in 40 °C thermostat water for 21 h. The battery was then maintained for 3 h at temperatures of 10, 20, 30, and 40 °C to measure the temperature change dV_0/dT of open-circuit voltage V_0. Fig. 6 compares the ΔS measured here with the previous data, with E_{emf} in Eq. (6) approximated by V_0. In the previous study, ΔS was positive near at SOC = 0.8. The temperature change of ΔS for the batteries used here, however, changed only slightly, but the ΔS averaged for temperature became negative across the entire range of SOC. Thus, entropy heat Q_S was exothermic during the discharge cycle and endothermic during the charge cycle.

4. Measurement of heat capacity and heat transfer coefficient

4.1. Measurement of battery heat capacity

Unlike in the previous study, this time the heat capacity of battery was measured using a twin-type calorimeter (SETARAM C-80) [7], increasing the battery temperature from 20 to 90 °C at a constant rate of 0.4 °C min^{-1}. The measured data was compensated for the lag in thermal response by assuming a first-order time constant [8]. After determination of the heat capacity of battery from the compensated thermal response in the range where the heat up rate was constant, the heat capacity C_{cell} could be approximated by a linear function of temperature as shown in Fig. 7.

$$C_{cell}\,(\mathrm{J/^\circ C}) = 35.12 + 0.048T\,(^\circ\mathrm{C}) \quad (15)$$

4.2. Measurement of heat transfer coefficient from battery to ambient air

Lead wires for charging and discharging are soldered to the battery, and they promote heat transfer much more than a battery without wires. In order to again accurately measure the heat transfer coefficient from the battery to ambient air, the temperature drop of the battery was measured in a similar way to the previous study, as detailed below. The battery was suspended

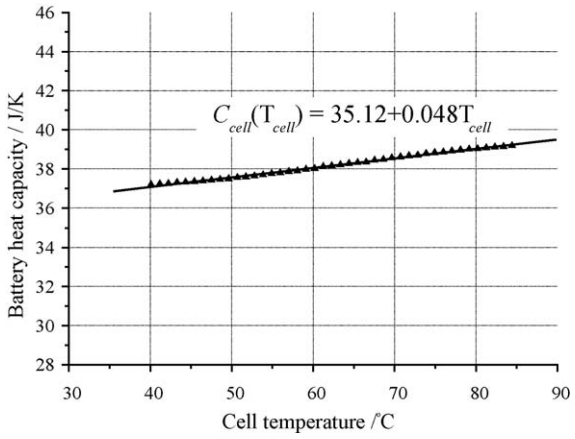

Fig. 7. Change of battery heat capacity by cell temperature.

in ambient air of constant temperature by the lead wires in a horizontal state, and cooled by natural convection, after being heated to 90 °C in a water thermostat. From the temperature drop data shown in Fig. 8, the heat transfer coefficient of the battery (including the lead wires) was measured for each divided temperature range from 10 to 80 °C. Comparing these measured values with the values from an arranged equation for heat transfer from a horizontal cylinder in air [9], we produced a correction factor for the lead-wire equipped batteries, as shown in Fig. 9.

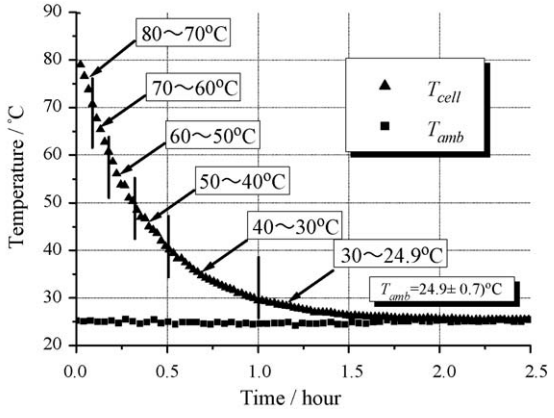

Fig. 8. Measured temperature drop of battery with lead wires.

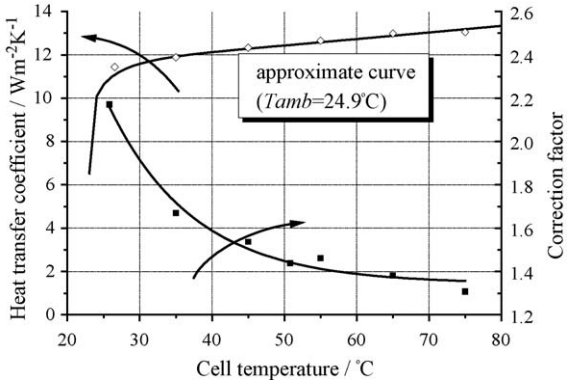

Fig. 9. Correction factor and measured heat transfer coefficient and its approximated curve.

This correction factor (■) is approximated by a solid line as shown in Fig. 9. The heat transfer coefficient for a pure horizontal cylinder was multiplied by the correction factor, and the heat transfer coefficient h for the real battery with lead wires could be approximated as shown by the upper solid line to match the measured value (◊).

5. Calculation of battery temperature rise and comparison with measured values

5.1. Inclusion of measured heat-source factors into analysis

In order to analyze thermal behavior of battery during charge and discharge cycles, the overpotential resistance to determine overpotential heat, the entropy change to determine entropy heat, the battery heat capacity, and the heat transfer coefficient from battery to ambient air were measured in the preceding sections. The overpotential resistance R_η was measured by four methods in Section 3.1. In the following analysis, the overpotential resistance $R(V–I)$ determined from the battery $V–I$ characteristics at 1C or less was primarily used as a function of battery temperature and SOC. The entropy change used in analysis was the temperature average value of the temperature change of open-circuit voltage V_0, which was approximated by a function of SOC. The battery heat capacity C_{cell} was approximated by a linear function of battery temperature (Eq. (15)). As done in our previous study [9] on a nickel-metal hydride battery, the heat transfer coefficient h was determined using a correction factor and a heat transfer equation, the later of which is a function of battery temperature T_{cell} and ambient temperature T_{amb}.

5.2. One-dimensional analysis of temperature distribution inside the battery

Fig. 10 shows the calculated results of radial distribution of battery temperature during discharge cycle of 3C for initial (ambient) temperature of 32.5 °C. One-dimensional calculations of radial temperature distribution were made by considering the current density distribution along current collection sheet as mentioned in Section 2.3. Between the cell center and the

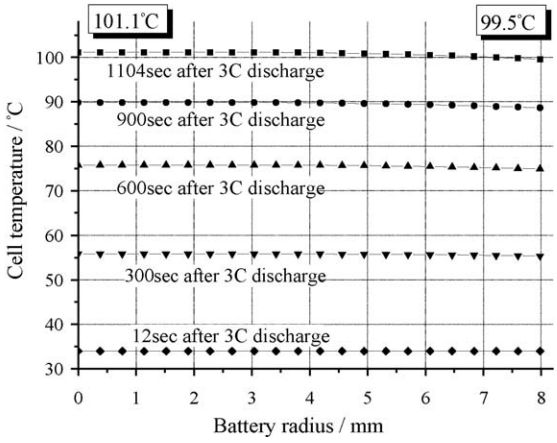

Fig. 10. Calculated radial distribution of cell temperature.

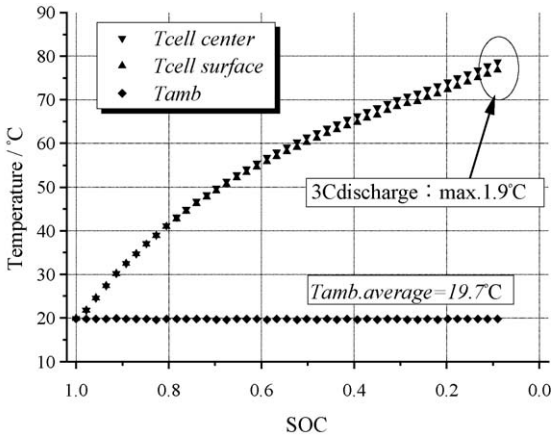

Fig. 11. Measured temperature of center and surface.

outer surface, a maximum temperature difference of 1.6 °C was calculated at the end of discharge. It was seen that internal temperature of battery was nearly uniform, even during rapid charge or discharge cycle with a current above the battery's rating. In other words, the surface temperature represents the battery temperature, and can be compared well with the temperature by Eq. (8) derived in the model of representative battery temperature. Furthermore, the difference in temperatures measured at battery center and surface during discharge cycle of 3C was 1.9 °C, as shown in Fig. 11, where the initial battery temperature is 19.7 °C. This temperature difference supports the calculated results.

5.3. Comparison of calculated and measured battery temperatures during rapid charge and discharge cycles

Fig. 12 compares the measured cell surface temperature with the temperature calculated by Eq. (8) for the representative battery temperature model using $R(V–I)$, and the surface temperature calculated by Eq. (14) for the radial temperature distribution model, during rapid charge/discharge cycles. Temperature of the charged/discharged battery was measured similarly to the previous study. A thermocouple of 0.1 mm wire diameter was soldered to the center of battery surface and measurements were taken with the batteries suspended in air by lead wires and cooled by natural convection.

Calculated temperatures for both rapid charge and discharge cycles were in good agreement with the measured values. Therefore, the representative cell temperature model presented herein can describe the thermal behavior of small batteries with minimal temperature distribution, such as those adopted here. However, during the charge/discharge cycles at or below 1C, the calculated value is a little smaller than the measured, and the calculated is a little larger than the measured during discharge cycle of 3C. Also, the calculated temperature during charge cycle of 1C showed a different trend of temperature increase from the measured. A root mean square deviation of temperatures calculated by $R(V–I)$ from measured temperatures was 1.0 °C for overall charge cycle, and 1.6 °C for overall discharge cycle. While battery temperature was calculated using R(OCV-CV) or R(60 s), the mean deviation was found to be higher than the above-stated values. Thus, $R(V–I)$ is the overpotential resistance that yields the most accurate estimation of battery temperature in the tested range of our study. In the future, these differences between calculation and measurement must be reduced further, and a method for predicting the thermal behavior of large batteries needs to be developed.

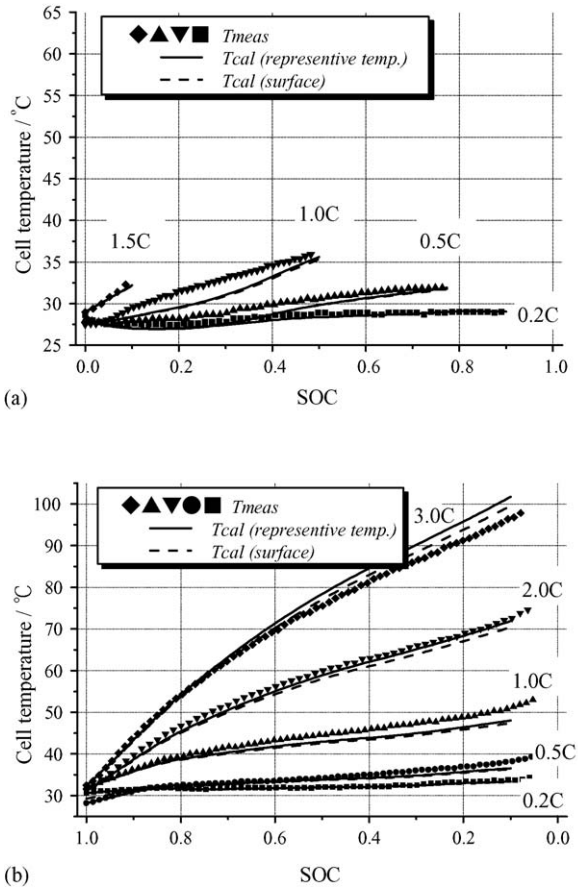

Fig. 12. Comparison of calculated and measured cell temperatures: (a) during charge; (b) during discharge.

6. Conclusion

Using small, commercially-available lithium-ion batteries, we have measured overpotential resistance, entropy change, battery heat capacity, and heat transfer coefficient to the ambient air from a battery attached with charge/discharge lead wires, which are needed to describe the battery thermal behavior. For overpotential resistance, the resistance by $V–I$ characteristics during constant-current charge/discharge cycle, the resistance by difference between open-circuit voltage and cell voltage, and the resistance by intermittent charge/discharge were mostly in good agreement. The resistance measured by AC impedance, however, was about half that in the above three methods. Using these measured results, we have analyzed the thermal behavior of battery during rapid charge and discharge cycles at up to three times larger current than the rated. The analysis was made with a

model using a representative battery temperature, and also with a model of radial temperature distribution. Battery temperature during rapid charge and discharge cycles was calculated using overpotential resistance determined from the *V–I* characteristics at the rated current or less. These calculated temperatures were compared with the measured battery temperatures, showing the calculated and the measured to be in good agreement. Furthermore, the difference in temperature between the battery center and surface was found to be small. The analysis methods presented here are thus effective for predicting the thermal behavior of small batteries.

Acknowledgements

We would like to express our gratitude to Drs. Kiyonami Takano and Yoshiyasu Saito of the National Institute of Advanced Industrial Science and Technology for their advice on measurement of battery heat capacity. Part of this research was supported by the 21st Century COE Program "Intelligent Human Sensing" from the ministry of Education, Culture, Sports, Science and Technology.

References

[1] T. Ozawa, K. Nozaki, Fuel cell and its application, Ohmu-sha, Tokyo, 1981.
[2] Electric Vehicle Handbook Editorial Committee, Electric Vehicle Handbook, Maruzen, Tokyo, 2001.
[3] K. Onda, H. Kameyama, T. Hanamoto, K. Ito, J. Electrochem. Soc 150 (2003) A285.
[4] Denchi-Binran Editorial Committee, Denchi-Binran, third ed., Maruzen, Tokyo, 2001.
[5] R. Tamamushi, Electrochemistry, second ed., Maruzen, Tokyo, 2000.
[6] K. Takano, T. Hirayama, T. Nakano, Bull. Electrotech. Lab. 60 (1996) 817.
[7] Y. Saito, K. Kanari, K. Takano, T. Masuda, Bull. Electrotech. Lab. 60 (1996) 763.
[8] Y. Saito, K. Takano, K. Kanari, T. Masuda, Bull. Electrotech. Lab. 60 (1996) 771.
[9] T. Araki, M. Nakavama, K. Fukuda, K. Onda, J. Electrochem. Soc. 152 (2005) A1128.